# Inner shell excitation of thiophene and thiolane: Gas, solid, and monolayer states

A. P. Hitchcock
*Department of Chemistry, McMaster University, Hamilton, Canada L8S 4M1*

J. A. Horsley
*Corporate Research Science Laboratories, Exxon Research and Engineering Company, Annandale, New Jersey 08801*

J. Stöhr
*IBM Almaden Research Center, San Jose, California 95120-6099*

(Received 9 May 1986; accepted 22 July 1986)

The electron energy loss spectra of gaseous thiophene and thiolane in the regions of S 2*p*, S 2*s*, and C 1*s* are presented along with the x-ray photoelectron yield (NEXAFS) spectra of both gases in the region of S 1*s* excitation. The thiophene spectra are compared to the corresponding NEXAFS spectra of solid (multilayer) and monolayer thiophene on Pt (111). MS-$X\alpha$ calculations of the C 1*s*, S 2*p*, and S 1*s* excitation spectra of free thiophene are also reported. Intercomparison of the gas, surface, and calculated spectra allows a complete interpretation of the spectral features and facilitates determination of the molecular orientation of thiophene with respect to the surface in both the compressed [thiophene on Pt (111) at 150 K] and relaxed [thiophene on Pt (111) at 180 K] monolayer phases.

## I. INTRODUCTION

Over the last few years inner shell excitation spectroscopies have proven to be useful for elucidating the unoccupied electronic structure of free and chemisorbed molecules. The combination of inner shell electron energy loss spectra (ISEELS)[1] of the gas, near edge x-ray absorption fine structure (NEXAFS) spectra[2] of the solid and oriented (monolayer) phases, and MS-$X\alpha$ calculations is proving to be particularly powerful for both spectral assignment and surface structure determination as exemplified by recent work on benzene and pyridine.[3] The polarization dependence of NEXAFS spectra[4] can provide a simple and powerful means of determining the orientation of a molecule with respect to the substrate in oriented multilayer solids or chemisorbed monolayers. In favorable cases, the position of $\sigma$ resonance features can be used to measure intramolecular bond lengths to chemically significant accuracy.[5]

The majority of inner shell excitation features of free molecules are one-electron promotions of core electrons to either Rydberg or unoccupied molecular orbitals. The large, diffuse Rydberg orbitals tend to collapse into the band structure of the solid upon chemisorption or solidification. Thus Rydberg orbitals can be identified readily by comparing gas and condensed phase spectra. The molecular orbitals can be classified as either $\pi^*$ or $\sigma^*$ according to their symmetry with respect to a particular bond axis or plane. When the orientation of a molecule is fixed, as in chemisorption or in an oriented multilayer, the symmetry of the state giving rise to a particular spectral feature can be identified from the polarization dependence of its spectral intensity.[4] Group theory provides the techniques to predict the polarization dependence for a given final state symmetry.

Recently, studies have been performed on inner shell excitation in noncyclic[6] and cyclic aliphatic hydrocarbons,[7] cyclic aromatics,[3] and nitrogen and oxygen heterocyclic compounds.[8] We have studied thiophene (thiofuran, $C_4H_4S$) and thiolane (thiacyclopentane, $C_4H_8S$) in order to extend our understanding of inner shell excitation phenomena in different environments and to investigate the utility of the sulfur and carbon inner shell spectra for determinating the electronic structure and carbon–sulfur bond lengths. This paper reports the C 1*s*, S 2*p*, and S 2*s* ISEELS and S 1s NEXAFS spectra of gaseous thiophene and thiolane along with the C 1*s* and S 2*p* NEXAFS of a multilayer solid and two monolayer phases of thiophene on a Pt (111) surface. MS-$X\alpha$ calculations of the C 1*s*, S 1*s*, and S 2*p* spectra of thiophene are also reported. Except for a very recent paper by Perera and LaVilla[9] reporting the S 1*s* photoabsorption spectrum of thiophene gas, the gas phase spectra have not been reported previously. The C 1*s* NEXAFS spectra of the two monolayer thiophene/Pt (111) phases have been reported earlier[10] and used, along with thermal desorption, x-ray photoemission, and vibrational electron energy loss data, to determine the structure, orientation, and chemical transformations of the surface adsorbed species as a function of temperature. The focus of this work is to obtain a full understanding of inner shell excitation in thiophene through comparisons of gas, solid, and monolayer thiophene spectra, comparison to thiolane, and with the assistance of the MS-$X\alpha$ results.

## II. EXPERIMENTAL

The experimental apparatus and techniques used to acquire the ISEELS spectra have been described in detail elsewhere.[6] Thiophene and thiolane (Aldrich, 99 + %) were thoroughly degassed prior to use. The absolute energy scales of the C 1*s* spectra were determined by calibrating with re-

 0021-9606/86/214835-14$02.10  

spect to the $1s \rightarrow \pi^*$ transition in $CO_2$ (290.7 eV[11]). The S 2*p* and S 2*s* spectra were calibrated with respect to the first feature of the C 1*s* spectrum.

The S 2*p* and C 1*s* NEXAFS spectra were acquired using the grasshopper monochromator on beam line I-1 at the Stanford Synchrotron Radiation Laboratory. The S 1*s* NEXAFS spectra of gaseous thiophene and thiolane were obtained with a double crystal monochromator [Si (111) crystals] on the VUV ring at the Brookhaven National Synchrotron Light Source. The procedure used to collect NEXAFS spectra in the partial electron yield mode has been described previously.[2,3] Both solid and monolayer spectra were measured on a Pt (111) crystal surface. The surface was cleaned by exposure to $10^{-7}$ Torr of oxygen at 870 K, followed by annealing at 1200 K in ultrahigh vacuum. Sulfur was removed by argon ion sputtering. Solid thiophene was prepared by dosing the Pt(111) crystal, kept at 100 K with $1 \times 10^{-7}$ Torr for 60 s (6 L). Two distinct monolayer phases were obtained by annealing this sample first to 150 and then to 180 K. The NEXAFS spectra of both phases were recorded with the crystal at 100 K. Based on an earlier analysis of the NEXAFS results,[10] the 150 K phase is believed to be a compressed monolayer with the thiophene rings oriented 40° with respect to the surface while the 180 K phase is a relaxed monolayer with the rings flat on the surface. Dramatic changes in the spectra were observed upon further heating above room temperature. The interpretation of these results in terms of changes in the chemisorption geometry and cleavage of the carbon–sulfur bond has been reported previously.[10]

## III. MULTIPLE SCATTERING CALCULATIONS OF THIOPHENE

X-ray absorption cross sections were calculated by the multiple scattering $X\alpha$ method following the approach of Dehmer and Dill,[12] as in our previous calculations on benzene.[3] The potential for thiophene was obtained by a MS-$X\alpha$ self-consistent calculation. The geometry used was that obtained by Bak *et al.*[13] by microwave spectroscopy. The effect of the core hole was taken into account by broken-symmetry transition state calculations with half an electron in the appropriate core orbital. Three sets of transition state calculations were performed, corresponding to 1*s* excitation of the two nonequivalent carbon atoms and of the sulfur atom. S 2*p* excitation was also calculated. Although this gave useful insight into spectral assignments, full details of the sulfur 2*p* edge absorption cross sections are not reported since the calculations were not able to take into account the spin-orbit splitting of the S 2*p* core hole. The muffin-tin sphere radii on the carbon atoms were chosen so that adjacent carbon spheres overlapped by 20%. The sulfur sphere radius was then adjusted to give 20% overlap with the two adjacent carbon spheres. Oscillator strengths for the bound state transitions were calculated by the method of Noodleman[14] using the appropriate core–hole transition state potential. The oscillator strengths were then converted to absorption cross sections following the method of Dehmer and Dill[12] using the relationship

$$\sigma(E) = \frac{\pi e^2 h}{mc} \cdot \frac{df}{dE} = \frac{\pi e^2 h}{mc} \cdot f \cdot \frac{dn}{dE},$$

where $f$ is the oscillator strength, $n$ is the principal quantum number, and $\sigma(E)$ is the peak height. The bound state resonances were represented by a Lorentzian line shape with a height of $\sigma(E)$ and a width $[(dn/dE)^{-1}]$ of 1 eV for carbon 1*s* and 1.5 eV for sulfur 1*s* features. These values were chosen to be close to the observed peak widths in the corresponding gas phase spectra, thus accounting for natural lifetime and vibrational broadening effects. Absorption cross sections for transitions to the continuum states were calculated using the program of Davenport.[15] For the continuum state calculations partial waves up to $l = 6$ were included for the outer sphere and up to $l = 2$ for the carbon and sulfur atoms. There was no significant difference in the results when the outer sphere was restricted to partial waves up to only $l = 5$. The calculated continuum cross sections were convoluted with a Lorentzian of 3 eV width, as in the benzene calculations,[3] to match the observed resonance width which presumably is related to molecular vibrations and the natural width associated with the short lifetime of the resonance states. The cross sections listed in Table III are per carbon 1*s* site and the calculated C 1*s* spectrum shown in Fig. 3 is the average of the calculated cross sections for the nonequivalent carbon atoms.

## IV. RESULTS AND DISCUSSION

### A. Thiophene

#### 1. Electronic Structure

In $C_{2v}$ symmetry, with the molecule in the *yz* plane, the core levels of thiophene are: $1a_1$ (S 1*s*), $[2a_1, 1b_2]$ ($C_{3,4}$ 1*s*); $[3a_1, 2b_2]$ ($C_{2,5}$ 1*s*); $4a_1$(S 2*s*), and $[5a_1, 1b_1, 3b_2]$ (S 2*p*). The four lowest energy unoccupied valence orbitals are $\pi^*$ ($4b_1$), $\sigma^*$(C–S) ($8b_2$), $\pi^*(2a_2)$, and $\sigma^*(12a_1)$. There are seven other unoccupied $\sigma^*$ valence levels in a minimal basis set description and transitions to some of these give rise to continuum features. However the majority of the features observed in the core spectra can be described in terms of one-electron transitions between the core and the three lowest energy $4b_1$, $8b_2$, and $2a_2$ unoccupied orbitals. The ordering of these three levels is predicted to be $4b_1 < 8b_2 < 2a_2$ by *ab initio* calculations[16] which also give the symmetries and energy orderings of the 13 occupied valence orbitals.[16,17] The symmetries of the states arising from core excitation to these three levels and the polarization of electric dipole transitions to these states are summarized in Table I.

The C 1*s*, S 2*p*, S 2*s*, and S 1*s* spectra of gaseous thiophene are presented in Fig. 1. Each spectrum is plotted on the same energy width and the spectra are positioned to align the C 1*s*, S $2p_{3/2}$, S 2*s*, and S 1*s* ionization potentials (I.P.'s). The solid bars before the hatched lines indicate the locations of the C 1*s* and S 2*p* I.P.'s as measured by XPS.[18] The S 2*s* and S 1*s* ionization potentials for gaseous thiophene have not been reported to our knowledge. Our estimates of these are indicated in Fig. 1 by the dashed lines before the hatched areas. The S 2*s* I.P. of solid thiophene is 228.6 eV.[19] The S $2p_{3/2}$ I.P. is 5.3 eV higher in the gas than in the solid while the gas–solid shift of the C 1*s* I.P. is 5.9 eV. Thus the S 2*s* I.P. of

TABLE I. Symmetry[a] and polarization of inner shell excited states in thiophene.

| Virtual valence level | | Excited state $\pi^*(4b_1)$ | | $\pi^*(2a_2)$ | | $\sigma^*(C\text{–}S)(8b_2)$ | |
|---|---|---|---|---|---|---|---|
| Core hole | | sym. | pol.[b] | sym. | pol. | sym. | pol. |
| C 1s | $a_1$ | $B_1$ | out | $A_2$ | $F$[c] | $B_2$ | in |
| | $b_2$ | $A_2$ | $F$[c] | $B_1$ | out | $A_1$ | in |
| S 2s | $a_1$ | $B_1$ | in | $A_2$ | $F$ | $B_2$ | in |
| S 1s | $a_1$ | $B_1$ | in | $A_2$ | $F$ | $B_2$ | in |
| S 2p | $a_1$ | $B_1$ | out | $A_2$ | $F$ | $B_2$ | in |
| | $b_1$ | $A_1$ | in | $B_2$ | in | $A_2$ | $F$ |
| | $b_2$ | $A_2$ | $F$ | $B_1$ | out | $A_1$ | in |

[a] The molecule is in the *yz* plane.

[b] Transitions from the $A_1$ ground state to $A_1$ and $B_2$ excited states are polarized *in*-plane and have maximum intensity when light is incident perpendicular to the plane of the ring (normal, 90°). Transitions to $B_1$ states are polarized *out*-of-plane and have maximum intensity when light is incident in the plane of the ring (glancing, 20°). Electric-dipole transitions to $A_2$ states are forbidden ($F$).

[c] The $C_{2v}$ symmetry of thiophene is broken in C 1*s* excitation assuming a localized C 1*s* hole so this selection rule may not be a rigid limitation.

gaseous thiophene is estimated to be 234.2(3) eV, 5.6(3) eV higher in the gas than in the solid. A S 1*s* I.P. of 2478.4(5) eV was estimated by assuming that the term value of the first feature is 5.0(5) eV, similar to those of 4.8(1) eV in the S 2*p* and 5.3(4) eV in the S 2*s* spectra. This estimate for the S 1*s* I.P. of thiophene is 0.8 eV higher than that estimated by Perera and LaVilla[9] from sulfur K fluorescence and photoelectron spectroscopy. The measured or estimated I.P.'s have been used to calculate term values for all of the spectral features. Term values ($T$ = I.P. − $E$) guide spectral assignments, particularly of the Rydberg transitions, since these have characteristic values depending on their symmetry.[20]

### 2. Carbon 1s spectra

The C 1*s* ISEELS spectrum of gaseous thiophene is compared to the C 1*s* NEXAFS spectra of the solid and two monolayer phases in Fig. 2. For each monolayer phase, spectra were recorded with the photon beam incident at 20° and 90° to the surface. The grazing incidence spectrum of the solid [multilayer on Pt(111)] (not shown) was essentially identical to the normal incidence spectrum. The energies and proposed assignments of the observed features are presented in Table II.

The first point to note is the great similarity of the solid and gas phase spectra. In addition, although the intensities vary in the spectra of the oriented monolayers because of polarization effects, the observed features occur at essentially the same energies as the features in the solid and gas phase spectra. This indicates that intramolecular transitions to a common set of final orbitals dominate the inner shell spectroscopy of thiophene in all phases. One difference between the monolayer and gas or solid phase spectra is that the onset of each of the monolayer C 1*s* spectra occurs around 283 eV, about 1.5 eV below the onset of the multilayer and gas phase spectra. The additional intensity on the low energy side of feature 1 in the monolayer spectra (shaded in Fig. 2) is attributed to transitions to unoccupied metal–molecule bands such that the 283 eV onset represents the Fermi level of the thiophene covered Pt(111) surface. In addition to the lowered threshold, the resonances below 290 eV are broadened considerably in the 180 K monolayer spectra. This is attributed to interactions between the molecular and the metal levels. These two aspects are the major modifications of the thiophene electronic structure by chemisorption bonding to the metal surface which are detectible in the C 1*s* spectra of the monolayer phases.

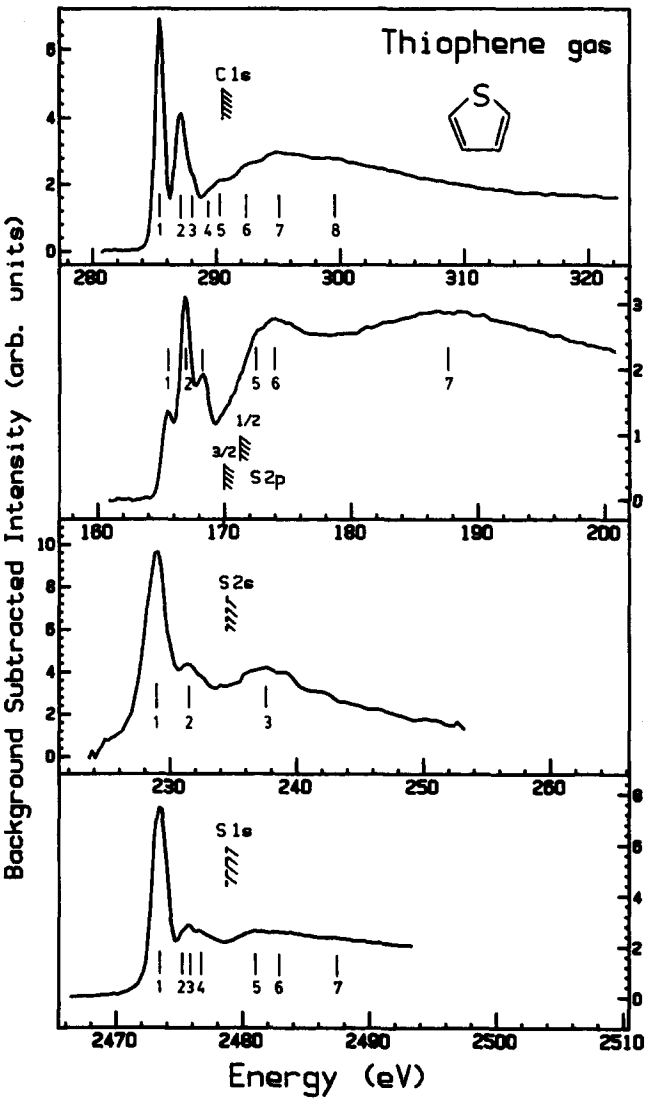


FIG. 1. The C 1*s*, S 2*p*, and S 2*s* spectra of thiophene recorded by ISEELS with 2.5 keV final electron energy and the S 1*s* NEXAFS spectrum of gaseous thiophene. The hatched lines indicate the locations of the ionization thresholds obtained from XPS for C 1*s* and S 2*p* and estimated as indicated in the text for S 2*s* and S 1*s*. All spectra have had a curved background subtracted. This background was visually estimated from the signal before the onset of core excitation features.

As with the closely related aromatic heterocycles furan and pyrrole,[8] four electric-dipole allowed C 1*s*→$\pi^*$ transitions are expected to contribute in the first several eV of the thiophene C 1*s* spectrum. The $C_{2,5}$ and $C_{3,4}$ carbon 1*s* levels of thiophene are estimated from XPS to be separated by 0.3 eV.[18] According to *ab initio* calculations[16] the $4b_1(\pi^*)$ and $2a_2(\pi^*)$ orbital energies differ by 2.3 eV while valence electronic spectroscopy[21] indicates that the $3b_1(\pi)\rightarrow 4b_1(\pi^*)$

TABLE II. Energies and proposed assignments of features in the carbon 1s spectrum of thiophene in the gas, solid, compressed monolayer [150 K on Pt(111)], and relaxed monolayer [180 K on Pt(111)] phases.

| | Gas | | Solid | Monolayer | | | | Assignment final orbital | |
|---|---|---|---|---|---|---|---|---|---|
| | $E$ | $T$[a] | $E$ | 150 K | | 180 K | | | |
| # | ±0.1 eV | eV | ±0.3 eV | 20° | 90° | 20° | 90° | $C_{2,5}$ | $C_{3,4}$ |
| 1 | 285.4[b] | 4.9 | 285.7 | 285.6 | 285.5 | 285.7 | 285 | $\pi^*(4b_1)$ | $\pi^*(4b_1)$ |
| 2 | 287.1 | 3.2 | 287.3 | 287.3 | 287.2 | ··· | 287.5 | $\sigma^*$(C–S) | $\pi^*(2a_2)$ |
| 3(sh) | 288.0 | 2.3 | ··· | (287.7) | (288.3) | ··· | (288.6) | 3p | |
| 4(sh) | 289.3 | 1.0 | 289.2 | ··· | ··· | (289.9) | ··· | 4p | |
| I.P. | 290.3[c] | | 285.0[d] | | | | | | |
| 5 | 290.4 | −0.1 | | 290.4 | 291.1 | ··· | 290.5 | | |
| 6 | 292.6 | −2.3 | 293.0 | 292.3 | 292.3 | ··· | 292.3 | $\sigma^*$(C–C) | |
| 7 | 294.9 | −4.6 | 296.2 | 295.5 | 296.1 | 295.3(2) | 295.7 | $\sigma^*$(C–C) | |
| 8 | 299(1) | −9 | 301(1) | 303(1) | 302(1) | 303(1) | 302(1) | shakeup | |

[a] $T$ = I.P. − $E$.

[b] Calibrated to be 5.34 eV lower than the C 1s→π* transition in $CO_2$ at 290.7 eV (Refs. 11 and 26).

[c] Average value. The I.P.'s of the two types of C 1s levels are 290.2(2) ($C_{3,4}$) and 290.5(2) eV ($C_{2,5}$) from XPS (Ref. 18).

[d] From XPS (Ref. 19). This value is relative to the Fermi energy of the Au substrate of the XPS spectrometer and the position relative to the Pt(111) substrate used in this work will differ. The onset at 284.2 eV which appears as a shoulder on the first peak of the C 1s NEXAFS of solid thiophene (Fig. 2) likely indicates the correct location of the ionization threshold relative to the Pt(111) fermi level.

and $3b_1(\pi)\rightarrow 2a_2(\pi^*)$ transitions of thiophene are separated by about 1.5 eV. In furan all four of the C 1s→π* transitions were resolved whereas only three could be distinguished by pyrrole.[8] Since the C 1s splittings decrease as the electronegativity decreases it should be even more difficult to distinguish all four features in thiophene. Based on the estimated separations quoted above the $\pi^*(4b_1)$–$\pi^*(2a_2)$ but not the $C_{2,5}$–$C_{3,4}$ splitting should be resolvable with our experimental resolution (approximately 0.6 eV in ISEELS and 1.0 eV in NEXAFS).

The lowest energy C 1s feature is assigned to C 1s $(a_1,b_1)\rightarrow\pi^*(4b_1)$ transitions from both the $C_{2,5}$ and $C_{3,4}$ core levels. All of these transitions are polarized in the plane of the ring and thus will have maximum intensity with x rays incident normal to the ring. From this assignment the orientation of the thiophene molecules with respect to the surface can be deduced from the polarization dependence of feature 1 in the spectra of the two monolayer phases. In both phases the first peak is strongest at grazing incidence and weaker (150 K) or absent (180 K) in the normal incidence monolayer spectra. This indicates that thiophene lies flat on the Pt(111) surface at 180 K. The residual π* intensity in the normal incidence 150 K spectrum indicates that thiophene does not lie flat on the surface at saturation coverage at this temperature but instead packs more closely by sitting tilted with respect to the surface. A detailed analysis of the polarization dependence at 150 K shows that the plane of the ring lies at 40° to the surface in this compressed monolayer phase.[10] Recently Sexton[30] has used vibrational energy loss and thermal desorption spectroscopy to deduce that thiophene adopts both compressed, tilted and flat, π-bonded phases when absorbed at low temperature on Cu(100). These are similar geometries to those we deduce from NEXAFS for thiophene on Pt(111).

On the basis of its energy the second feature in the C 1s spectrum suggests assignment to the C $1s\rightarrow\pi^*(2a_2)$ transition. However, the second spectral feature is most intense at normal incidence in the monolayer spectra, a polarization dependence opposite to that of the first peak. Thus the second feature is attributed primarily to C 1s→σ*(C–S) $(8b_2)$ transitions. Previously the $Z$ dependence of the correlation between bond lengths and the energies of σ* transitions relative to the I.P. ($\delta = E - \text{I.P.} = -T$) has indicated that transitions to σ* states shift to lower energy as the atomic number of the bonded atoms increases.[5] Thus the σ*(C–S) feature is expected to lie below the I.P., consistent with our assignment of feature 2 to transitions to this level.

In the 180 K relaxed monolayer phase both the $\pi^*(4b_1)$ and σ*(C–S) $(8b_2)$ transitions are appreciably broadened because of bonding interactions with the surface. By contrast, the first few features in the 150 K monolayer spectra are not much broader than their counterparts in the gas or multilayer spectra. This suggests that there is very little interaction between the metal surface and the π* or σ* (C–S) levels, further supporting the proposed tilted geometry in the 150 K phase.

Several weak features are observed between the σ*(C–S) transition and the I.P. in the gas phase spectrum. These are not observed in the solid state spectrum which is consistent with their assignment to 3p (#3) and 4p (#4) Rydberg transitions as suggested by their term values.[20]

The absolute C 1s photoabsorption cross section (on a per carbon atom basis) calculated by MS-$X\alpha$ is shown in Fig. 3 in comparison to the gas phase spectrum. For this plot the discrete and continuum transitions have been broadened by 1 and 3 eV Lorentzians, respectively. The calculated transition energies relative to the $C_{3,4}$ I.P., and the calculated peak cross sections are summarized in Table III. According to the MS-$X\alpha$ calculations there should be two peaks below the I.P. (Rydberg states were not calculated). The first peak corresponds to overlapping $C_{2,5}$ and $C_{3,4}$ $1s\rightarrow\pi^*(4b_1)$ transitions, which are calculated to be separated by only 0.06 eV.

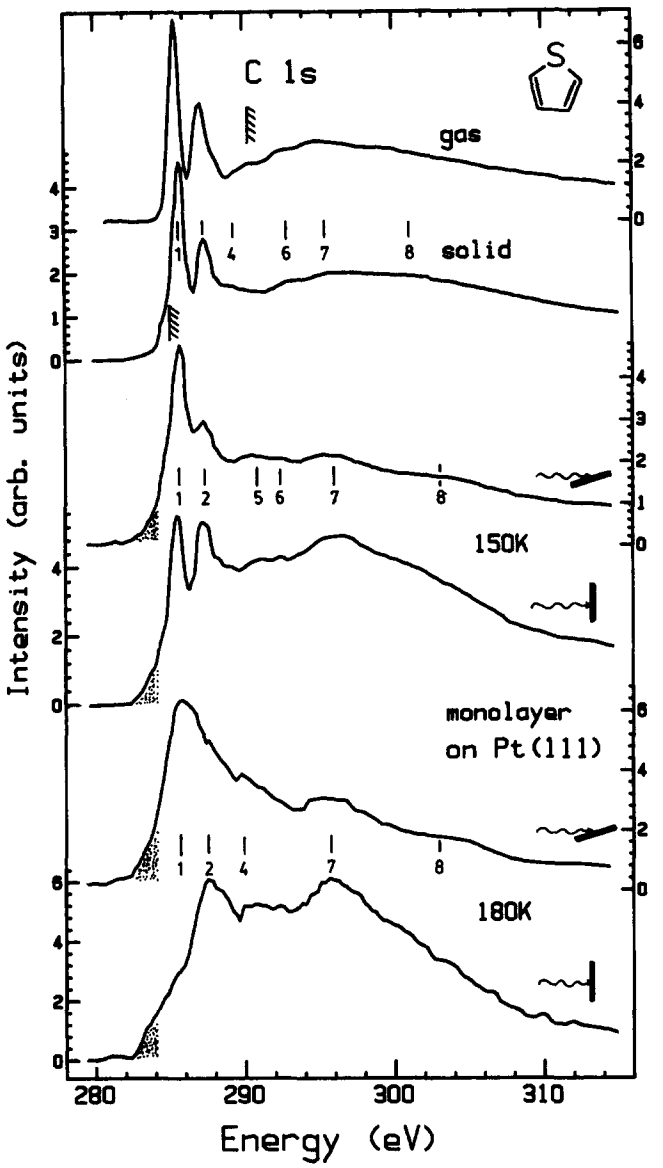


FIG. 2. The background subtracted C 1s spectra of thiophene in the gas (ISEELS), solid, and monolayer (NEXAFS) phases. The NEXAFS spectra were recorded with both 20° and 90° photon incidence on both the compressed (150 K) and relaxed (180 K) monolayer phases. The hatched lines indicate the location of the C 1s ionization thresholds. The highlighted area below 284 eV indicates signal observed in the monolayer but not the gas or solid spectra.

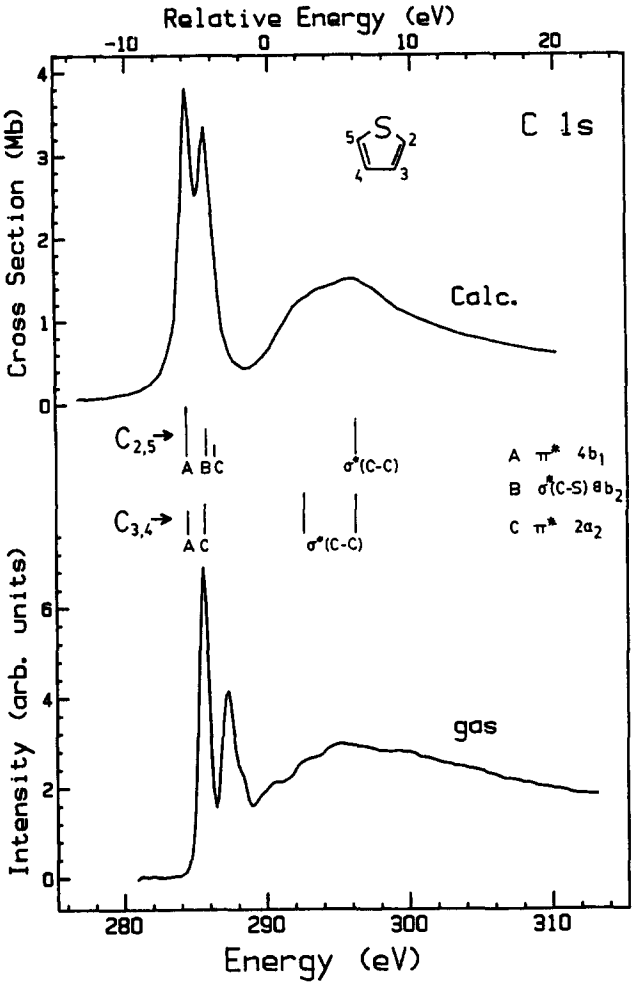


FIG. 3. Comparison of the calculated and experimental gas phase carbon 1s spectra of thiophene. The calculated spectrum has been shifted so that the ionization threshold matches experiment. States calculated below the I.P. have been broadened by a 1 eV Lorentzian, those above the I.P. with a 3 eV Lorentzian. The scale for the calculated cross section refers to the value per carbon atom, averaged over the $C_{2,5}$ and $C_{3,4}$ sites.

The second peak is more complex. Most of the intensity comes from two overlapping transitions: the $C_{2,5}$ $1s\rightarrow\sigma^*(C\text{–}S)(8b_2)$ transition (for which there is no $C_{3,4}$ 1s counterpart) and the $C_{3,4}$ $1s\rightarrow\pi^*(2a_2)$ transition. The $C_{2,5}$ $1s\rightarrow\pi^*(2a_2)$ transition is very weak and lies 0.67 eV *above* the corresponding $C_{3,4}$ $1s\rightarrow\pi^*(2a_2)$ transition. The total intensity in the C $1s\rightarrow\pi^*(2a_2)$ transition (summed over the nonequivalent carbons) is much less than the total intensity in the C $1s\rightarrow\pi^*(4b_1)$ transition, because of the different contributions of the $C_{2,5}$ excitations. The lower intensity of the $C_{3,4}$ $1s\rightarrow\pi^*(4b_1)$ compared to the $C_{2,5}$ $1s\rightarrow\pi^*(4b_1)$ transition reflects the spatial distribution of the $4b_1$ orbital, which is appreciably localized at the heteroatom end of the molecule.[22] A similar effect is seen in the relative intensities of the $\pi^*(4b_1)$ resonances in furan and pyrrole[8] where the larger $C_{3,4}$–$C_{2,5}$ splitting allowed the relative intensities of the transitions from each carbon site to the $\pi^*(4b_1)$ orbital to be determined experimentally. In the carbon 1s spectrum of furan two peaks of roughly equal intensity are observed in the region where the $C_{2,5}$ $1s\rightarrow\pi^*(2a_2)$ and $C_{3,4}$ $1s\rightarrow\pi^*(2a_2)$ transitions are expected. The roughly equal intensity of these two transitions in furan is consistent with MO calculations which indicate a fairly uniform spatial distribution of the $\pi^*(2a_2)$ orbital on the four carbon atoms.[22] The present MS-$X\alpha$ calculations suggest that the $\pi^*(2a_2)$ orbital of thiophene is much more localized on the $C_{3,4}$ carbons than its counterpart in furan or pyrrole.

The two calculated peaks (Fig. 3) obviously correspond to features 1 and 2 in the experimental carbon 1s spectra. The calculations therefore suggest that feature 2 arises from overlapping $C_{2,5}$ $1s\rightarrow\sigma^*(C\text{–}S)(8b_2)$ and $C_{3,4}$ $1s\rightarrow\pi^*(2a_2)$ transitions with approximately equal contributions. The experimentally determined separation of the $2a_2$ and $4b_1$ C $1s\rightarrow\pi^*$ states is approximately 2.7 eV according to our assignments. This value is similar to the difference in the virtual M.O. energies predicted by *ab initio* calculation[16] although it is somewhat larger than the separation of 1.5 eV for

TABLE III. Relative energies and cross sections calculated by MS-$X\alpha$ for C 1$s$ and S 1$s$ photoabsorption of thiophene.

| Term values[a] eV | Peak cross section[b] Mb | Transition |
|---|---|---|
| Carbon 1$s$ | | |
| +5.90 | 4.41 | $C_{2,5}$ $1s\rightarrow\pi^*(4b_1)$ |
| +5.84 | 2.46 | $C_{3,4}$ $1s\rightarrow\pi^*(4b_1)$ |
| +4.57 | 2.89 | $C_{3,4}$ $1s\rightarrow\pi^*(2a_2)$ |
| +4.50 | 2.66 | $C_{2,5}$ $1s\rightarrow\sigma^*$(C–S)$(8b_2)$ |
| +3.90 | 0.72 | $C_{2,5}$ $1s\rightarrow\pi^*(2a_2)$ |
| −2.25 | ...[c] | $C_{3,4}$ $1s\rightarrow\sigma^*$(C–C) |
| −6.00 | ...[c] | $C_{3,4}$, $C_{2,5}$ $1s\rightarrow\sigma^*$(C–C) |
| Sulfur 1$s$ | | |
| +5.91 | 0.122 | S $1s\rightarrow\pi^*(4b_1)$ |
| +5.20 | 0.337 | S $1s\rightarrow\sigma^*$(C–S)$(8b_2)$ |
| −2.00 | ...[c] | S $1s\rightarrow\sigma^*$(C–C) |
| −6.75 | ...[c] | S $1s\rightarrow\sigma^*$(C–C) |

[a]Energy relative to the $C_{3,4}$ I.P. According to XPS the $C_{3,4}$ and $C_{2,5}$ I.P.s differ by only 0.3 eV (Ref. 18).

[b]Cross section per carbon atom for each transition. In Fig. 3 the average cross section is plotted (i.e., half the sum of the $C_{2,5}$ and $C_{3,4}$ cross sections listed in this table).

[c]Peak cross sections for the $\sigma^*$ continuum states are not meaningful because of the broadening imposed ( a 3 eV Lorentzian). The positions of the resonances were taken from the unbroadened results.

the corresponding valence shell $\pi\rightarrow\pi^*$ states of thiophene.[21] A similar increase from valence to core excitation in the separation of the transitions to the $\pi^*$ levels was observed in furan and pyrrole.[8]

Above 290 eV the C 1$s$ spectra of all phases show a broad maximum around 296 eV with several shoulders. These features are strongest in the normal incidence monolayer spectrum indicating that they arise from in-plane transitions to final states of $\sigma$ symmetry. The MS-$X\alpha$ calculations (Fig. 3, Table III) show two continuum resonances, a weak one at 2.25 eV above the I.P. with a $C_{3,4}$ component only, and a strong resonance at 6.0 eV above the I.P. with components from both $C_{3,4}$ and $C_{2,5}$ excitation. The strong resonance evidently corresponds to the 296 eV feature observed most clearly in the gas phase and normal incidence monolayer spectra (feature 7). There is also a weak feature (#6) at 2.3 eV above the I.P. in the gas phase and monolayer spectra which the calculations suggest should be assigned to a $\sigma^*$ resonance. There are no calculated resonances in the region 6–20 eV above the I.P. The weak, broad feature (#8) observed at 9 eV above the I.P. in the gas phase spectrum is apparently not a $\sigma^*$ resonance according to the calculations. In addition, this feature appears to shift about 4 or 5 eV to higher energy in the monolayer spectra, while the other continuum features do not shift between phases. Finally, the intensity of feature 8 relative to feature 7 is greater in the glancing than in the normal incidence monolayer spectra, which is inconsistent with a $\sigma$ symmetry final state. Feature 8 may correspond to a double excitation of $\pi$ symmetry or a shakeup continuum. Neither of these types of processes would be reproduced in the one-electron MS-$X\alpha$ calculations. Alternatively it could be a one-electron transition which is not reproduced in the calculations.

The previously reported correlation between bond length and $\sigma$ resonance position[5] predicts that only two features should be observed at 7.2 and 10.1 eV above the I.P., corresponding to the two C–C bond lengths of 142.3 and 137.0 pm,[23] respectively. However the $\sigma^*$(C–C) levels are delocalized around the ring and thus a 1:1 correlation between the observed resonances and a particular bond is probably unrealistic. Rather we expect that the intensity weighted average position of the continuum resonances will agree with the position predicted from the correlation based on the average C–C bond length in thiophene (139 pm). The center of the $\sigma^*$(C–C) resonance intensity can be estimated most easily from the normal incidence 180 K monolayer spectrum. The position of 296 eV observed in this spectrum is somewhat lower than the position of 298 eV predicted from the average bond length of 139 pm. The present results are consistent with other recent work[3,8] which suggests that the simple correlation[5] has to be modified to average over several observed continuum resonances in those cases where the $\sigma^*$ states are delocalized over several bonds. This appears to be particularly important in molecules such as cyclic aromatics. The delocalized nature of the $\sigma^*$ states in aromatic species means that the position of any single observed resonance does not correlate with a particular bond length. The complication to the bond length correlation caused by split $\sigma^*$ resonances appears to be less severe in thiophene than in furan or pyrrole.[8] This can be attributed to the fact that the $\sigma^*$(C–S) level is at much lower energy and thus does not interact appreciably with the $\sigma^*$(C–C) levels whereas the $\sigma^*$(C–O) and $\sigma^*$(C–N) levels in furan and pyrrole are at a similar energy to the $\sigma^*$(C–C) levels and thus mix strongly with them.

It is clear that a correlation between continuum resonance position and molecular structure exists even in cases where the $\sigma^*$ intensity is distributed over several delocalized states. This can be noted in the present work both in the reasonable agreement of the mean resonance position with the predicted position based on average bond length and also in terms of the more rapid decrease in the C 1$s$ continuum intensity of thiolane compared to that of thiophene (see Fig. 8). The additional intensity at high energy in the thiophene C 1$s$ continuum is associated with $\sigma^*$(C–C) levels which reflect the shorter C–C bond length of the unsaturated species.

### 3. Sulfur 2s and 1s spectra

The S 2$s$ ISEELS and S 1$s$ NEXAFS spectra of gaseous thiophene are shown in Fig. 1 while the energies and assignments of the observed features are listed in Table IV. The S 1$s$ spectrum of thiophene has been reported very recently, in addition to the sulfur K fluorescence spectrum and MO calculations.[9] The energies and proposed assignments from this work are also listed in Table IV for ease of comparison. Our S 1$s$ spectrum is in excellent agreement with that of Perera and LaVilla.[9] All features occur at the same energy within the measurement uncertainties and with similar relative intensities. However our interpretation of the S 1$s$ spectral features differs significantly, as discussed below.

The S 1$s$ and S 2$s$ spectra are remarkably similar, as

TABLE IV. Energies and proposed assignments for features observed in the S 2*s* and S 1*s* spectra of gaseous thiophene.

S 2*s* (ISEELS)

| # | *E* ± 0.3 eV | *T* ± 0.5 eV | Assignment (final orbital) |
|---|---|---|---|
| 1 | 228.9 | 5.3 | $\pi^*(4b_1)$,$\sigma^*$(C–S)$(8b_2)$ |
| 2 | 231.3 | 2.9 | 4*p* |
| I.P. | 234.2(3)[a] | | |
| 3 | 237(1) | −3 | $\sigma^*$(C–C) |

S 1*s* (NEXAFS)

| | This work | | Ref. 9 | | |
|---|---|---|---|---|---|
| # | *E* ± 0.3 eV | *T* ± 0.5 eV | *E* eV | (Assignment) | Assignment (this work) (final orbital) |
| 1 | 2473.4 | 5.0 | 2473.0 | [$\pi^*(4b_1)$] | $\pi^*(4b_1)$,$\sigma^*$(C–S)$(8b_2)$ |
| 2(sh) | 2475.1 | 3.3 | ... | | 4*s* |
| 3 | 2475.6 | 2.8 | 2475.4 | [$\pi^*(2a_2)$] | 4*p* |
| 4(sh) | 2476.3 | 2.1 | 2476.9 | [$\sigma^*$(C–S)$(8b_2)$] ($12a_1$) | 5*p* |
| I.P. | 2478.4(5)[b] | | 2477.6[c] | | |
| 5 | 2480.8 | −2.4 | 2481 | | $\sigma^*$(C–C) |
| 6 | 2482.5 | −4.1 | 2482 | | $\sigma^*$(C–C) |
| 7 | 2487(1) | −9 | 2488 | | shakeup |

[a] Estimated from the S 2*s* I.P. of solid thiophene (228.6 eV) (Ref. 19) and the average of the solid–gas shifts in the C 1*s* (5.3 eV) and S 2*p* (5.9 eV) I.P.s.

[b] Estimated by fixing the term value of feature 1 to be the average of the values in the C 1*s*, S 2*p*, and S 2*s* spectra. For comparison the S 1*s* I.P.'s of gaseous $CH_3SCH_3$ and $CH_3SH$ are 2477.6 and 2478.0 eV (Ref. 28).

[c] This value was estimated from the S 1*s* fluorescence spectrum and photoelectron spectroscopic data (Ref. 9).

expected since the originating orbital of the transitions is on the same atom of the molecule and has the same symmetry and similar spatial extent. The term values for feature 1 derived with our estimated I.P.'s are 5.0 and 5.3 eV, respectively, in the S 1*s* and S 2*s* spectra, consistent with assignment of the first feature to transitions to the $\pi^*(4b_1)$ level. The S $ns\rightarrow\pi^*(2a_2)$ ($n = 1$ or 2) transitions are symmetry forbidden. The alignment of the *second* feature in the S 2*s* and the S 1*s* spectra with the $\sigma^*$(C–S) peak in the C 1*s* spectrum suggests assignment of these features to transitions to the $\sigma^*$(C–S)$(8b_2)$ level. This is the interpretation proposed by Perera and LaVilla[9] based on a frozen orbital approximation and the ordering of the virtual levels in the MNDO and *ab initio* (STO-3G) calculations. However, we do not believe this to be correct since, based on the spatial localization of the core levels, the $\sigma^*$(C–S) transition should be at least as strong relative to the $\pi^*(4b_1)$ transition as in the C 1*s* spectrum. The MS-$X\alpha$ calculation resolves these difficulties and provides a guide to the correct assignment.

The absolute S 1*s* photoabsorption cross section calculated by MS-$X\alpha$ is shown in Fig. 4 in comparison to the gas phase spectrum. For this plot the discrete and continuum transitions have been broadened by 1.5 and 3 eV Lorentzians, respectively. The transition energies, which are calculated relative to the I.P., are summarized in Table IV along with the calculated cross sections. The calculated intensities are in excellent agreement with those reported by Perera and LaVilla.[9] According to our MS-$X\alpha$ results the S $1s\rightarrow\sigma^*$(C–S)$(8b_2)$ and S $1s\rightarrow\pi^*(4b_1)$ transitions occur at essentially the same energy. This indicates that *both* transitions should be assigned to feature 1 in the S 2*s* and S 1*s* spectra. The S $ns\rightarrow\sigma^*$(C–S) transition is expected to be strong because of the localization of the upper level on the sulfur atom. The S $ns\rightarrow\pi^*(4b_1)$ transition is relatively intense because of the considerable aromatic character of thiophene and thus appreciable delocalization of the $\pi^*(4b_1)$ level onto the sulphur.

We attribute the additional weak features in the discrete portion of the S 1*s* and S 2*s* spectra to Rydberg transitions and assign them according to their term values.[20] (Note that the Rydberg numbering scheme for the sulfur core spectra differs by 1 in *n* value from that in the carbon 1*s* spectrum, since the S 3*s* and S 3*p* orbitals are valence.) This differs from the assignments of Perera and LaVilla,[9] who suggest that these features are associated with S 1*s* excitations to $2a_2$, $8b_2$, and $12a_1$ unoccupied MO levels. The absence of these transitions in the MS-$X\alpha$ calculations; the arguments presented above in favor of assigning S $1s\rightarrow\sigma^*$(C–S)$(8b_2)$ transitions to peak 1, and the forbidden character of the S $1s(a_1)\rightarrow\pi^*(2a_2)$ transition all support our interpretation. All of the S 2*s* features are considerably broader than the corresponding features in the S 1*s* spectrum because of the very short lifetime of the S 2*s* hole associated with the rapid Coster–Kronig ($L_1L_3L_3$ Auger) decay.

The continuum features observed about 3 eV above the S 2*s* and S 1*s* ionization thresholds are attributed to S $ns\rightarrow\sigma^*$(C–C) transitions. The MS-$X\alpha$ calculation of the S 1*s* continuum predicts two resonances at 2.0 and 6.75 eV above the I.P. The positions of these resonances relative to the I.P. are very similar to the calculated positions of the two

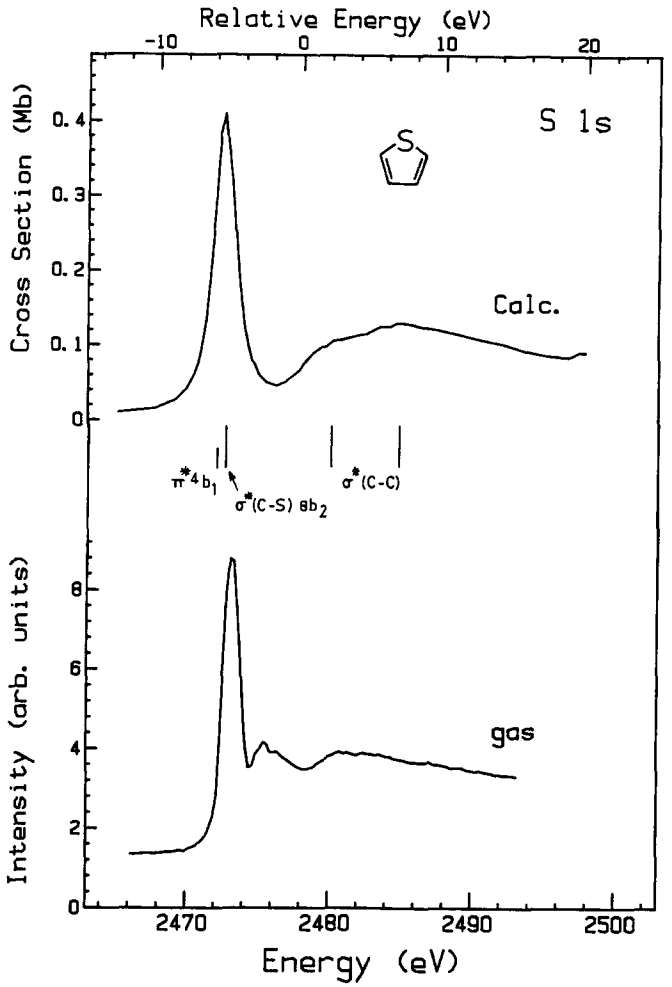


FIG. 4. Comparison of the calculated and experimental gas phase sulfur 1*s* spectra of thiophene. The calculated spectrum has been shifted so that the ionization threshold matches experiment. States calculated below the I.P. have been broadened by a 1.5 eV Lorentzian, those above the I.P. with a 3 eV Lorentzian.

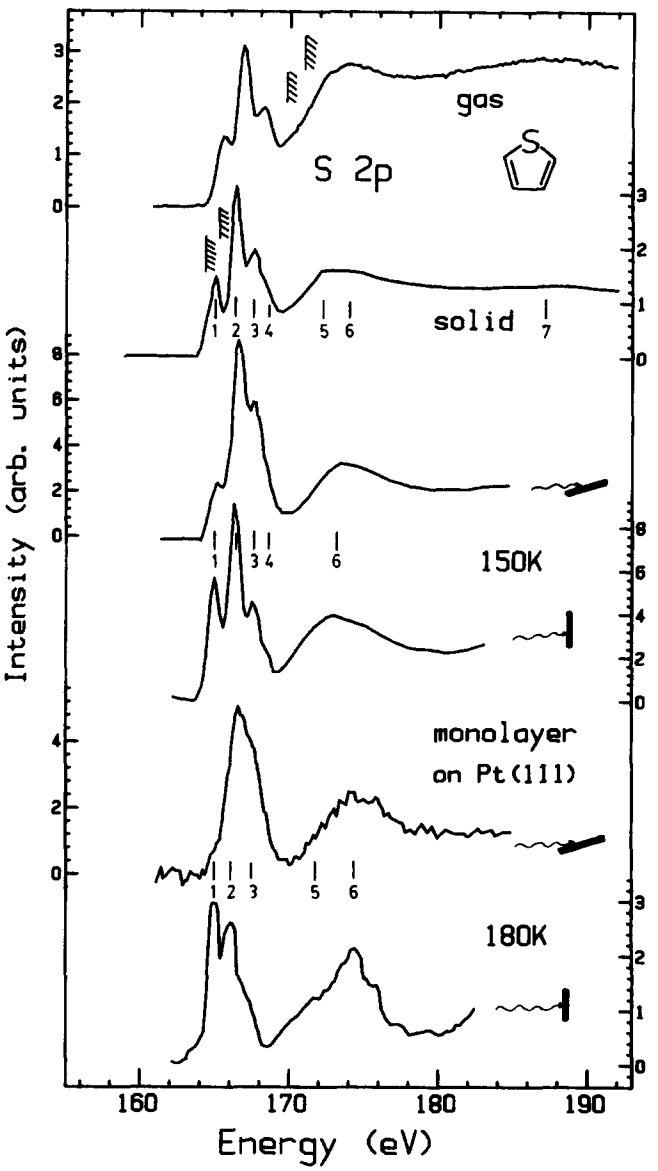


FIG. 5. The background subtracted S 2*p* spectra of thiophene in the gas (ISEELS), solid, and monolayer (NEXAFS) phases. The NEXAFS spectra were recorded with both 20° and 90° photon incidence on both the compressed (150 K) and the relaxed (180 K) monolayer. The hatched lines indicate the location of the S 2*p* ionization thresholds.

$\sigma^*$ resonances in the carbon 1*s* spectrum. There are no calculated resonances in the region 6–20 eV above the I.P. The calculations suggest that features 5 and 6 in the gas phase S 1*s* spectrum correspond to $\sigma^*$ continuum resonances with feature 7 possibly corresponding to a shakeup continuum. The similarity in the positions of the $\sigma^*$ resonances (relative to the I.P.) at the S 1*s* and C 1*s* edges suggests that the upper levels for the transitions are the same for both edges corresponding to states delocalized over the entire ring. The sulfur component or the carbon component of these levels is populated, depending on the atomic site of the initial core level. $\sigma^*$ states delocalized on the heteroatom also occur in furan and pyrrole since transitions to $\sigma^*$(C–C) levels are observed in the O and N 1*s* spectra.[8] Further support for a $\sigma^*$(C–C) assignment is provided by comparison to the S 2*s* and S 1*s* spectra of thiolane (Fig. 7, Table VI, and Fig. 8) where the corresponding continuum features are observed several eV closer to threshold, consistent with the $\sigma$ resonance, bond length correlation, and the longer average C–C bond in thiolane (150 vs 139 pm).

An alternative possibility that was considered but rejected was assignment of these continuum features to S *ns*→S 3*d* transitions. This is not unreasonable since these features are also aligned with the first of the much more intense S 2*p*→3*d* continuum features. Although S *ns*→3*d* transitions are symmetry forbidden in atomic sulfur, they are allowed in thiophene and thus could be observed, albeit weakly. However the MS-$X\alpha$ results and comparison with the spectra of other heterocyclics[8] leads us to prefer the aforementioned $\sigma^*$(C–C) assignment.

### 4. Sulfur 2p spectra

The S 2*p* ISEELS spectrum of gaseous thiophene is compared to the NEXAFS spectra of the multilayer solid, and both the compressed monolayer [Pt(111) at 150 K] and relaxed monolayer [Pt(111) at 180 K] phases in Fig. 5. For each monolayer phase, spectra recorded with the photon beam incident at 20° and 90° to the surface are shown. Curved backgrounds estimated from the underlying continuum have been subtracted from all spectra and the mono-

TABLE V. Energies and proposed assignments of features in the sulfur $2p$ spectrum of thiophene in the gas, solid, compressed monolayer [150 K on Pt(111)] and relaxed monolayer [180 K on Pt(111)] phases.

| | Gas | | | Solid | Monolayer | | | | | |
|---|---|---|---|---|---|---|---|---|---|---|
| | $E$ | $T$[a] | | | 150 K | | 180 K | | Assignment | |
| # | ±0.1 eV | ±0.3 eV | | ±0.3 eV | 20° | 90° | 20° | 90° | Final orbital | |
| | | 3/2 | 1/2 | | | | | | 3/2 | 1/2 |
| 1 | 165.6 | 4.3 | | 165.1 | 165.0 | 165.0 | ... | 165.0 | $\sigma^*$(C–S)($8b_2$) | |
| 2 | 166.9[b] | 3.0 | 4.2 | 166.7 | 166.6 | 166.5 | 166.6 | 166.1 | $\pi^*(2a_2)$ | $\sigma^*$(C–S)($8b_2$) |
| 3 | 168.4 | 1.5 | 2.7 | 168.0 | 167.6 | 166.7 | 167.8 | 167.1 | $\sigma^*(12a_1)$ | $\pi^*(2a_2)$ |
| 4(sh) | 168.9 | | 2.2 | 168.9 | 168.3 | 168.3 | ... | ... | | $\sigma^*(12a_1)$ |
| 3/2 I.P. | 169.9(2)[c] | | | 164.3[d] | | | | | | |
| 1/2 I.P. | 171.1(2)[c] | | | 165.3[d] | | | | | | |
| 5 | 172.3 | | −2.0 | 172.4 | ... | ... | ... | 171.7 | $\sigma^*$(C–C) | |
| 6 | 173.9 | | −3.3 | 173.9 | 173.3 | 172.8 | 174.4 | 174.3 | S $3d$("$t_{2g}$") | |
| 7 | 187(1) | | −17 | 187(1) | ... | ... | ... | ... | S $3d$("$e_g$") | |

[a] $T$ = I.P. − $E$, as measured with respect to the indicated ionization threshold.
[b] Calibration at 6.3(1) eV below the S $2p_{1/2}\rightarrow 6a_{1g}$ transition in $SF_6$ [173.20 eV (Ref. 29)].
[c] From XPS (Ref. 18).
[d] From XPS (Ref. 19). A value of 163.8 eV ($2p_{3/2}$) has also been reported (Ref. 25).

layer data has been subjected to several three-point smooths. The grazing incidence spectrum of the solid [multilayer on Pt(111)] (not shown) was identical to the normal incidence spectrum of the solid. The energies and proposed assignments of the observed features are presented in Table V. As in the C $1s$ spectra the solid and gas phase S $2p$ spectra are quite similar indicating that transitions to the same intramolecular final states are occurring in all phases. There is a systematic shift of about 0.4 eV to lower energy in the condensed phase spectra. However this is believed to be an error in the monochromator calibration for the NEXAFS measurements. An expanded presentation of the structure between 164 and 170 eV is shown in Fig. 6. For this plot the condensed phase spectra have been shifted to remove the suggested calibration error and thus to align the 166.9 eV feature in all spectra. With this correction the main features in the S $2p$ spectra of all phases are in good alignment. A more significant difference is that the intensity of the discrete [$\pi^*$ and $\sigma^*$(C–S)] features relative to the continuum is considerably less in the gas than in the condensed phase spectra. The origin of this difference is not known.

The S $2p$ ion core is spin-orbit split into $2p_{3/2}$ and $2p_{1/2}$ components and thus the observed spectrum will be the superposition of two sets of transitions displaced by 1.2 eV.[24] As indicated in Table I, the S $2p\rightarrow\pi^*(4b_1)$ and S $2p\rightarrow\pi^*(2a_2)$ transitions each contain components with both in-ring and out-of-ring polarization. Thus the intensities of S $2p\rightarrow\pi^*$ transitions are expected to change relatively little with different angles of x-ray incidence. On the other hand both of the allowed S $2p\rightarrow\sigma^*$(C–S)($8b_2$) transitions are in-ring polarized and thus will exhibit strong intensity variation, with maximum intensity at normal incidence for the 180 K monolayer phase where the rings are parallel to the surface. The first peak in the S $2p$ spectrum of 180 K monolayer thiophene is very intense at normal incidence and weak or absent at glancing incidence. This behavior clearly indicates that feature 1 is the S $2p_{3/2}\rightarrow\sigma^*$(C–S)($8b_2$) transition. A similar although attenuated polarization is observed for feature 1 in the 150 K monolayer spectrum, consistent with this assignment and the proposed tilted geometry in this phase.[10] It appears that the expected lowest energy S $2p_{3/2}\rightarrow\pi^*(4b_1)$ transition is very weak. The second feature in the normal incidence 180 K monolayer spectrum is relatively sharp and is attributed to the S $2p_{1/2}\rightarrow\sigma^*$(C–S)($8b_2$) spin-orbit partner to feature 1. There is considerable intensity at the energy of feature 2 in all of the glancing incidence spectra. This indicates that the S $2p_{3/2}\rightarrow\pi^*(2a_2)$ transition is also contributing. The third feature in the spectrum (around 168 eV) is assigned to S $2p_{1/2}\rightarrow\pi^*(2a_2)$ transitions. Since S $2p\rightarrow\pi^*(2a_2)$ excitations generate states with both in-ring and out-of-ring polarization (see Table I), one expects little change in the intensity of features 2 and 3 with x-ray incidence angle, as observed.

The MS-$X\alpha$ calculations of the oscillator strengths for S $2p$ excitations, although nonrelativistic, do give support to the proposed assignments. According to the calculations, the S $2p\rightarrow\sigma^*$(C–S)($8b_2$) excitation is much stronger than any other transition. The $8b_2$ orbital was calculated to have 28% sulfur $d$ character and 22% sulfur $p$ character, the remainder being mainly carbon $2p$. In contrast, the $\pi^*(4b_1)$ and $\sigma^*(2a_2)$ orbitals were calculated to have only 4% sulfur $d$ character. In addition, the calculations predict a diffuse $\sigma^*$ level of $a_1$ symmetry with significant (5%) sulfur $d$ character lying just above the $\sigma^*(2a_2)$ level. The relative intensities of the S $2p$ transitions follow the percentage $d$ character of the upper states. Thus the S $2p\rightarrow\pi^*(4b_1)$ transition is calculated to lie 0.7 eV below the S $2p\rightarrow\sigma^*(8b_2)$ transition but it has an order of magnitude lower intensity. The calculations support the assignment of feature 1 to predominantly the S $2p_{3/2}\rightarrow\sigma^*$(C–S)($8b_2$) transition. Transitions to the $\pi^*(2a_2)$ and $\sigma^*(12a_1)$ levels also have some intensity and will contribute to features 2 and 3.

The S $2p$ continuum (Fig. 5) shows broad features around 3 and 17 eV above the edge. These arise from transi-

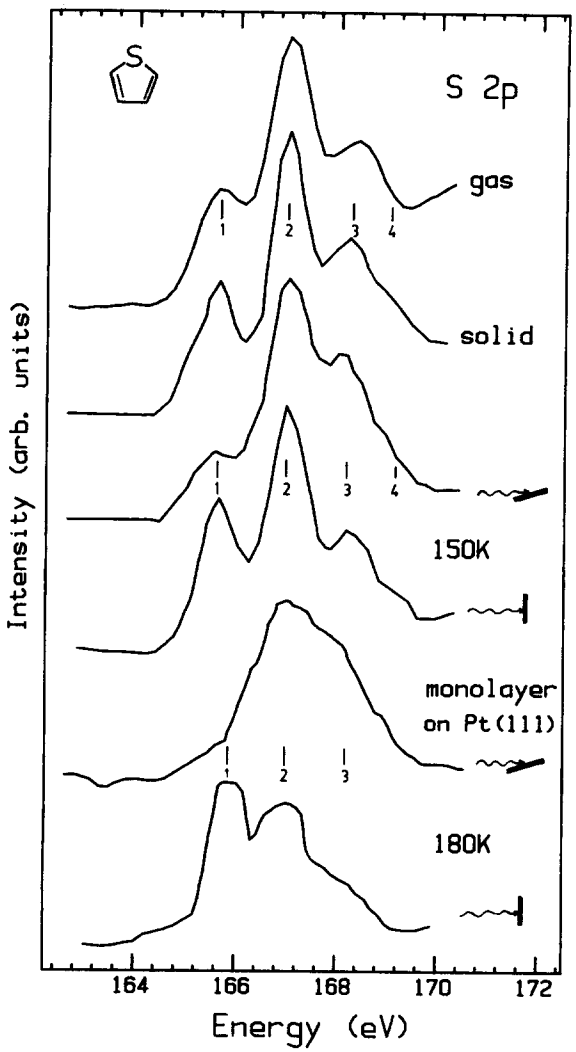


FIG. 6. An expanded plot of the S 2*p* spectra of thiophene shown in Fig. 5. The condensed phase spectra have been shifted 0.4 eV to align them with the gas phase spectrum at the 166.9 eV feature.

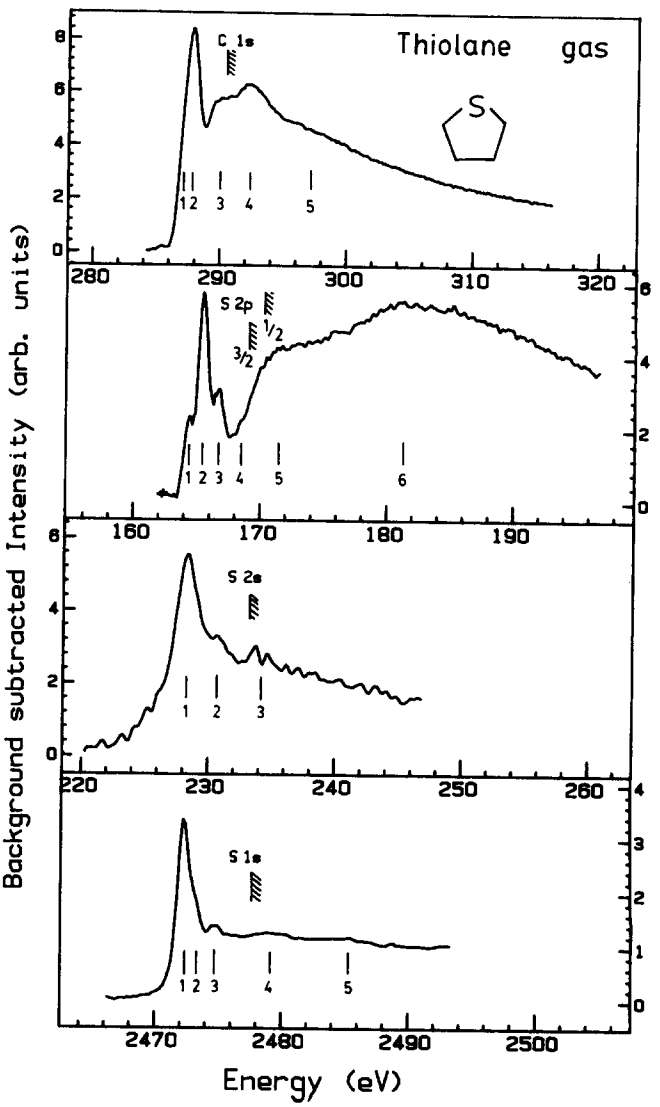


FIG. 7. The C 1*s*, S 2*p*, and S 2*s* spectra of *thiolane* recorded by ISEELS with 2.5 keV final electron energy and the S 1*s* NEXAFS spectrum of gaseous thiolane. The hatched lines indicate the estimated locations of the ionization thresholds.

tions to atomic S 3*d* levels. Corresponding features are seen in many S 2*p* spectra. The first broad peak (at 174 eV) has a shoulder at 172.3 eV, about 2 eV above the average S 2*p* I.P. This probably arises from transitions to the lower energy, delocalized $\sigma^*$(C–C) level. This feature can be detected in the normal incidence 180 K relaxed monolayer spectrum but not at glancing incidence, consistent with its assignment to transitions to an in-plane $\sigma^*$ level. The S 2*p* excitation to the second delocalized $\sigma^*$(C–C) level is expected about 5 eV above the I.P. and thus will be masked to a greater extent by the first S 3*d* resonance.

## B. Thiolane

### *1. Gas phase spectra*

The C 1*s*, S 2*p*, S 2*s* ISEELS and S 1*s* NEXAFS spectra of gaseous thiolane are presented in Fig. 7. Each spectrum is plotted on the same energy width and the spectra are positioned to align the first transition. The energies, term values, and proposed assignments are listed in Table VI. The hatched lines in Fig. 7 indicate the locations of the ionization thresholds, which are all estimated since XPS spectra of gaseous thiolane have not been reported to our knowledge. The average C 1s I.P.s of the saturated heterocyclics, tetrahydrofuran, and pyrrolidine, have been estimated to be 0.4 eV higher than the average C 1*s* I.P.'s of their aromatic counterparts, furan and pyrrole.[8] Thus an average C 1*s* I.P. of 290.5(3) eV is estimated for thiolane. The separation of the I.P.'s of the two C 1*s* environments is expected to be 0.3(1) eV, as measured in the gas phase for thiophene[18] and in the solid state for thiolane.[24] This is too small to generate observable splittings in the ISEELS spectra although it will contribute to broadening of the features. The heteroatom *K*-shell I.P.'s of the O and N analogs decrease by 1.0 and 1.5 eV, respectively, between the unsaturated and saturated species.[8] Thus the sulfur core I.P.s of thiolane are estimated to be 0.6(4) eV smaller than those of thiophene. Based on these estimates the shifts in both the heteroatom and C 1*s* I.P.'s between the aliphatic and the aromatic heterocyclic species agree within 0.3 eV with those reported in the solid state.[25]

TABLE VI. Energies and proposed assignments for features observed in the C 1*s*, S 2*p*, S 2*s*, and S 1*s* spectra of gaseous thiolane.

C 1*s* (ISEELS)

| # | *E* ± 0.1 eV | *T* eV | Assignment (final orbital) |
|---|---|---|---|
| 1(sh) | 287.1(3) | 3.4(4) | $\pi^*(CH_2)$ |
| 2 | 287.8[a] | 2.7 | $\sigma^*$(C–S) |
| 3 | 290.0 | 0.5 | Rydberg |
| I.P. | 290.5(5)[b] | | |
| 4 | 292.3 | −1.8 | $\sigma^*$(C–C) |
| 5 | 297(2) | −6 | $\sigma^*$(C–C) |

S 2*p* (ISEELS)

| # | *E* ± 0.1 eV | *T* ± 0.6 eV | | Assignment (final orbital) | |
|---|---|---|---|---|---|
| | | 3/2 | 1/2 | 3/2 | 1/2 |
| 1 | 164.4 | 4.9 | - | $\sigma^*$(C–S) | |
| 2 | 165.5[c] | 3.8 | 5.0 | $\pi^*(CH_2)$ | $\sigma^*$(C–S) |
| 3 | 166.7 | 1.6. | 3.8 | | $\pi^*(CH_2)$ |
| 4 | 168.5 | 0.8 | 2.0 | | Ryd. |
| 3/2 I.P. | 169.3(6)[d] | | | | |
| 1/2 I.P. | 170.5(6)[d] | | | | |
| 5 | 172(2) | −2 | | $\sigma^*$(C–C),S 3*d* | |
| 6 | 181(1) | −11 | | S 3*d* | |

S 2*s* (ISEELS) and S 1*s* (NEXAFS)

| S 2*s* | | | S 1*s* | | | |
|---|---|---|---|---|---|---|
| # | *E* ± 0.3 eV | *T* ± 0.8 eV | # | *E* ± 0.3 eV | *T* ± 0.8 eV | Assignment (final orbital) |
| 1 | 228.3 | 5.3 | 1 | 2472.3 | 5.5 | $\sigma^*$(C–S) |
| | | | 2(sh) | 2473.1 | 4.7 | $\pi^*(CH_2)$ |
| 2 | 230.8 | 2.8 | 3 | 2474.7 | 3.1 | 3*p* |
| I.P. | 233.6(6)[e] | | I.P. | 2477.8(6)[e] | | |
| 3 | 234(1) | 0 | 4 | 2479(2) | −1 | $\sigma^*$(C–C) |
| | | | 5 | 2485(2) | −7 | $\sigma^*$(C–C) |

[a] Calibrated at 2.9(1) eV below the C 1*s*→$\pi^*$ transition in $CO_2$ [290.7 eV (Refs. 11 and 26)].
[b] Estimated from the C 1*s* I.P. of thiophene. The splitting of the C 1*s* levels is 0.3(1) eV (Ref. 24).
[c] Calibration at 7.72(8) eV below the S $2p_{1/2}$→$6a_{1g}$ transition in $SF_6$ [173.20 eV (Ref. 29)].
[d] Estimated from the S 2*p* I.P. of thiophene, the separation of the I.P.'s of solid thiophene and thiolane (Ref. 25), and extrapolation from the I.P.'s of O and N heterocyclics (Ref. 8).
[e] Estimated. See the text and footnote (d) of this table for details.

### 2. Carbon 1s spectrum of thiolane

In comparison to thiophene several changes are expected in the carbon 1*s* spectrum of thiolane. First since thiolane is saturated, $\pi^*(C=C)$ transitions cannot occur and thus the C 1*s*→$\sigma^*$(C–S) is expected to be the dominant transition to a virtual valence level below the I.P. Second, the $\sigma^*$(C–C) resonance intensity in the continuum should appear markedly closer to threshold according to the bond length correlation since the thiolane (C–C) bond is 153 pm long, 14 pm longer than the average C–C bond length in thiophene. Third, the C 1*s*→$\sigma^*$(C–S) transition might shift to lower term value since the C–S bond is 12 pm longer in thiolane than in thiophene.

The main peak at 287.8 eV in the C 1*s* spectrum is assigned to transitions to the $\sigma^*$(C–S)($8b_2$) level. Interestingly there is very little change in the term value of this feature relative to that of the corresponding $\sigma^*$(C–S) transition in thiophene. This is clearly illustrated in the direct comparison of the thiophene and thiolane C 1*s* spectra presented in Fig. 8, which also compares the S 2*p* and S 1*s* spectra of these two species. Note that the energy scales in Fig. 8 refer to the thiophene spectra. All of the thiolane spectra have been shifted to align the $\sigma^*$(C–S) features with those in thiophene. With this presentation the positions of the thiolane I.P.'s (appropriately corrected for the energy shift) approximately match those of thiophene. The similarity of the term values for $\sigma^*$(C–S) excitations in thiophene and thiolane suggests that the energies of C 1*s*→$\sigma^*$(C–S) resonances are relatively insensitive to the length of the C–S bond, in sharp contrast to the situation for $\sigma^*$(C–C), $\sigma^*$(C–N), and $\sigma^*$(C–O) resonances. This is disappointing with regard to the use of NEXAFS for C–S bond length determination but it is not entirely unexpected since the $\sigma$ resonance shifts to lower energy and the bond length sensitivity decreases with heavier atoms (higher *Z* parameter) according to the results presented earlier.[5]

Relative to the continuum the feature assigned as the $\sigma^*$(C–S) transition in thiolane appears to be somewhat stronger than that in thiophene (Fig. 8). This suggests that there is a second contribution to the 287.8 eV peak in thio-

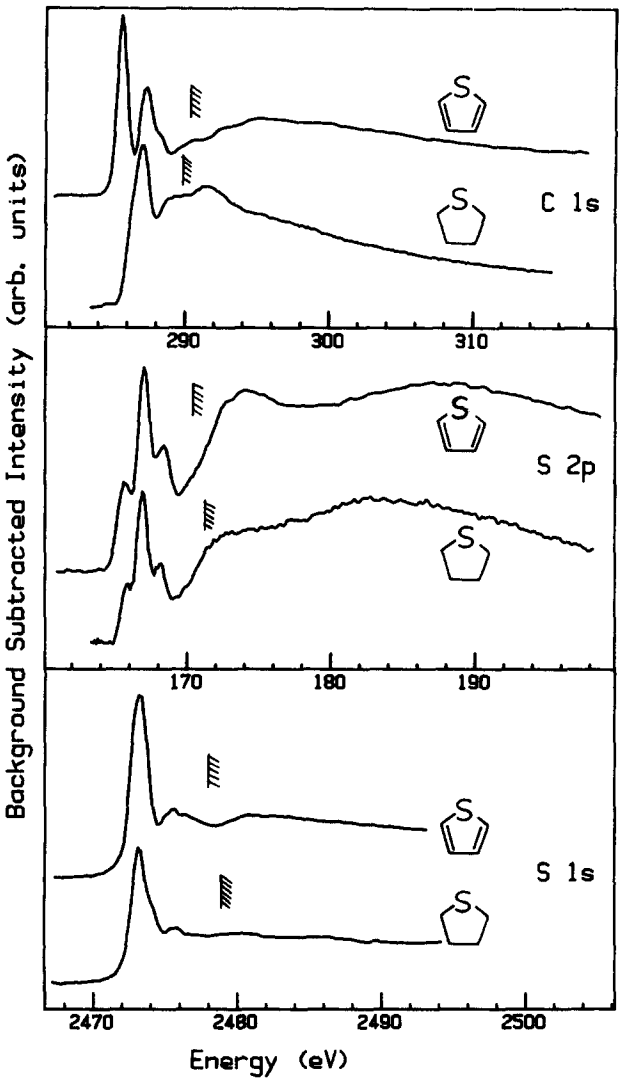


FIG. 8. Comparison of the C 1*s*, S 2*p*, and S 1*s* spectra of gaseous thiophene and thiolane. The energy scales shown are accurate for thophene. The thiolane spectra have been shifted by $-0.7$ eV (C 1*s*), $+1.4$ eV (S 2*p*), and $+1.1$ eV (S 1*s*), respectively, to align the $\sigma^*$(C–S) features with those of thiophene. The thiolane I.P.s indicated are located correctly with respect to the thiolane spectra (i.e., they are on a shifted energy scale).

lane. Close examination of the spectrum reveals a shoulder (labeled #1) on the low energy side at about 287.1 eV which we assign to transitions to a $\pi^*(CH_2)$ level. Features attributed to $\pi^*(CH_2)$ transitions are observed about 3 eV below the I.P. in tetrahydrofuran, pyrrolidine, and piperidine[8] as well as in a wide range of cyclic[7] and noncyclic[26] alkanes. It is possible that the relative ordering of the $\sigma^*$(C–S) and $\pi^*(CH_2)$ transitions should be reversed from that indicated above and in Table VI. This would make the term value of the C $1s\rightarrow\sigma^*$(C–S) transition in thiolane 0.2 eV larger than that in thiophene, consistent with the relative positions of the S $2p\rightarrow\sigma^*$(C–S) and S $1s\rightarrow\sigma^*$(C–S) transitions in thiophene and thiolane (see below) and also with the fact that the increased C–S bond length in thiolane should shift the $\sigma^*$(C–S) feature to lower energy at least to some extent. The broad structure (#3) centered around 290 eV is attributed to unresolved, overlapping Rydberg transitions converging on the I.P.

The peak at 292.3 eV in the C 1*s* continuum (#4) is attributed to the $\sigma^*$(C–C) shape resonance. Its location ($\delta = 1.8$ eV) is in good agreement with that predicted from the bond length correlation ($\delta = 1.3$ eV) based on the C–C bond length of thiolane (153.2 pm[23]). Above this feature there is a weak, broad maximum at 297 eV (#5) with an onset around 294 eV. Features similar to this are observed consistently in the C 1*s* spectra of saturated cyclic[8] and noncyclic[26] alkanes. In these spectra they were interpreted as one-electron transitions to $\sigma^*$ states rather than to multielectron processes such as double excitation or shakeup. Peak 5 is far too broad ($\sim$4 eV half-width) to be a double excitation. Shakeup features can be identified by the correspondence between the energy of their onsets and the positions of XPS shakeup satellites. For thiolane a weak shakeup peak is observed about 6.2 eV above the main line in the XPS spectrum of the solid.[25] This is several eV higher in energy than the onset of peak 5 relative to the I.P. Thus, as in the other saturated hetrocyclic compounds[8] and saturated alkanes,[7,26] the highest energy continuum feature is attributed to a one-electron transition to a $\sigma^*$ state. It appears that even in aliphatic compounds, transitions occur to more $\sigma^*$ states than are predicted within the most simple interpretation of the bond length correlation.[5] However the transition which correlates with the nearest neighbor bond length dominates the spectra of saturated species to a greater extent than in the spectra of aromatics.

### 3. Sulfur 2p spectrum of thiolane

The S 2*p* spectrum of thiolane is remarkably similar to that of thiophene (see Fig. 8). This is very surprising at first sight since the unoccupied electronic structure of these two molecules differs considerably. There is a shift to lower energy in going from thiophene to thiolane but the term values of the individual features in each molecule are quite similar since there is a shift of about the same amount in the S 2*p* I.P.'s according to our estimates. Table VI summarizes our assignments of the thiolane S 2*p* spectral features to overlapping transitions to $\sigma^*$(C–S) and $\pi^*(CH_2)$ levels with $2p_{3/2}$ and $2p_{1/2}$ core holes. The similarity of the S 2*p* spectrum of thiolane to that of thiophene can be explained by the negligible contribution of S $2p\rightarrow\pi^*(C=C)(4b_1)$ transitions in thiophene and the substitution of S $2p\rightarrow\pi^*(CH_2)$ transitions in thiolane for the S $2p\rightarrow\pi^*(C=C)(2a_2)$ transitions in thiophene. The occurrence of transitions from the localized S 2*p* core level to an orbital formally labeled $\pi^*(CH_2)$ is reasonable since O $1s\rightarrow\pi^*(CH_2)$ and N $1s\rightarrow\pi^*(CH_2)$ transitions are clearly observed in the spectra of tetrahydrofuran and pyrrolidine,[8] molecules where there is no overlapping, low lying $\sigma^*$ level. The similarity of the thiophene and thiolane spectra may also be a consequence of contributions to the thiolane spectrum from excitations to a $\sigma^*(a_1)$ level with an appreciable S 3*d* component, similar to that which the MS-$X\alpha$ calculation suggests occurs in thiophene.

The two maxima in the S 2*p* continuum (#5,6) are associated with the S 3*d* resonances, as are those in the thiophene S 2*p* continuum. Each of these maxima are closer to the I.P. in thiolane than the corresponding maxima in thiophene (see Fig. 8). This is consistent with the general obser-

vation that continuum resonances shift to lower energy with increasing bond length. Recently, similar shifts in the positions of Si $2p \rightarrow 3d$ resonances in a number of Si compounds have been documented and correlated to bond lengths.[27] The S $2p$ continuum of thiolane is weaker in the first 5 eV above threshold than that of thiophene. This suggests less contribution from S $2p \rightarrow \sigma^*$(C–C) transitions in thiolane than in thiophene. This is consistent with $\sigma^*$(C–C) levels being more localized in noncyclic aliphatic than in aromatic molecules.

### *4. Sulfur 1s and 2s spectra of thiolane*

Aside from additional broadening in the S $2s$ spectrum associated with the rapid Coster–Kronig decay, the S $2s$ ISEELS and S $1s$ NEXAFS spectra of gaseous thiolane (shown in the lower two panels of Fig. 7) are very similar. The first feature is attributed to transitions to the $\sigma^*$(C–S) level. As with the S $2p \rightarrow \sigma^*$(C–S) transitions, the term values for the S $ns \rightarrow \sigma^*$(C–S) features (derived with estimated I.P.'s) are about 2 eV larger than that of the $\sigma^*$(C–S) feature in the C $1s$ spectrum. A similar shift in the $\sigma^*$(C–S) term value between the C $1s$ and S $1s$, $2s$, and $2p$ spectra is also observed in thiophene. This observation is a good example of the limitations of a simple, frozen orbital approximation to the interpretation of core excitation spectra. Additional features observed below the I.P.'s are assigned to transitions to $\pi^*(CH_2)$ and Rydberg states according to their term values. The weak peaks in the continuum of each spectrum (#3 in S $2s$, #4 and #5 in S $1s$) likely arise from transitions to that portion of the delocalized $\sigma^*$(C–C) levels which overlap the sulfur atom. As expected these features are much weaker in the sulfur inner shell spectra than in the carbon $1s$ spectrum of thiolane. Also, they are weaker than the corresponding S $ns \rightarrow \sigma^*$(C–C) transitions in thiophene, providing further evidence for the greater localization of the $\sigma^*$(C–C) orbital in thiolane than thiophene. The comparison of the thiophene and thiolane S $1s$ spectra (Fig. 8) gives further support to our assignments. Although the spectral shapes are roughly similar the main peak ($\sim$2473 eV) is about 20% less intense relative to the continuum in thiolane than in thiophene. This is due to the additional contribution in thiophene of the S $1s \rightarrow \pi^*(4b_1)$ transition at this energy. According to the MS-$X\alpha$ calculation (Table III) the $\pi^*(4b_1)$ contribution is about 25% of the total, in good agreement with the decrease in intensity of feature 1 from thiophene to thiolane.

## V. CONCLUSIONS

The inner shell spectra of thiophene and thiolane in the gas phase; and thiophene in the solid and two monolayer phases have been reported and analyzed with the aid of MS-$X\alpha$ calculations. Comparison of all these results has allowed the development of a rather complete picture of the inner shell excitation spectroscopy of these molecules and has substantiated the previous interpretation of the NEXAFS spectra in terms of particular molecular orientations of thiophene in the two low temperature monolayer phases on the Pt(111) surface.[10] Prominent transitions to $\sigma^*$(C–S) states occur below the I.P. in all core spectra. The $\sigma^*$(C–S) resonance position is found to be relatively insensitive to the C–S bond length in contrast to the position of the S $3d$ resonances in the S $2p$ continuum or the $\sigma^*$(C–C) resonances observed in the near continuum of all the core spectra. The positions of the latter two classes of features shift systematically with the differences in the C–S and C–C bond lengths between thiophene and thiolane, consistent with the previously documented bond length–resonance position correlation.[5]

## ACKNOWLEDGMENTS

This work was supported in part by grants from the Natural Sciences and Engineering Research Council of Canada (NSERC). We thank Dave Newbury, Dr. I. Ishii, and Phil Fischer for assistance in the ISEELS calibration and data manipulation. APH acknowledges the support of an NSERC University Research Fellowship. The assistance of F. Sette and A. L. Johnson in recording the S $2p$ and C $1s$ NEXAFS spectra of thiophene is gratefully acknowledged. The S $1s$ spectra were recorded in collaboration with F. Zaera, G. M. Watson, and J. B. Hastings, who we would like to thank for making the data available. Portions of this work were done at SSRL (Stanford) and NSLS (Brookhaven). Both of these facilities are supported by the Office of Basic Energy Sciences at DOE and the Division of Materials Research of NSF.

[1] C. E. Brion, S. Daviel, R. N. S. Sodhi, and A. P. Hitchcock, AIP Conference Proceedings **94**, 426 (1982); A. P. Hitchcock, J. Electron Spectrosc. Relat. Phenom. **25**, 245 (1982).
[2] J. Stöhr in *Chemistry and Physics of Solid Surfaces*, edited by R. Vaneslow and R. Howe (Springer, Berlin, 1984), Vol. V, p. 231.
[3] J. A. Horsley, J. Stöhr, A. P. Hitchcock, D. C. Newbury, A. L. Johnson, and F. Sette, J. Chem. Phys. **83**, 6099 (1985).
[4] J. Stöhr and R. Jaeger, Phys. Rev. B **26**, 4111 (1982).
[5] F. Sette, J. Stöhr, and A. P. Hitchcock, J. Chem. Phys. **81**, 4906 (1984).
[6] A. P. Hitchcock, S. Beaulieu, T. Steel, J. Stöhr, and F. Sette, J. Chem. Phys. **80**, 3927 (1984).
[7] A. P. Hitchcock, D. C. Newbury, I. Ishii, J. Stöhr, J. A. Horsley, R. D. Redwing, A. L. Johnson, and F. Sette, J. Chem. Phys. **85**, 4849 (1986).
[8] D. C. Newbury, I. Ishii, and A. P. Hitchcock, Can. J. Chem. **64**, 1145 (1986).
[9] R. C. C. Perera and R. E. LaVilla, J. Chem. Phys. **84**, 4228 (1986).
[10] J. Stöhr, J. L. Gland, E. B. Kollin, R. J. Koestner, A. L. Johnson, E. L. Muetterties, and F. Sette, Phys. Rev. Lett. **53**, 2161 (1984).
[11] G. R. Wight and C. E. Brion, J. Electron Spectrosc. Relat. Phenom. **3**, 191 (1974).
[12] J. L. Dehmer and D. Dill, J. Chem. Phys. **65**, 5327 (1976).
[13] B. Bak, D. Christensen, L. Hansen-Nyggard, and J. Rastrup-Andersen, J. Mol. Spectrosc. **7**, 58 (1961).
[14] L. Noodleman, J. Chem. Phys. **64**, 2343 (1976).
[15] J. W. Davenport, Phys. Rev. Lett. **36**, 945 (1976).
[16] W. von Niessen, W. P. Kraemer, and L. S. Cederbaum, J. Electron Spectrosc. Relat. Phenom. **8**, 179 (1976).
[17] G. DeAlti and P. Decleva, Chem. Phys. Lett. **77**, 413 (1981).
[18] U. Gelius, C. J. Allan, G. Johansson, H. Siegbahn, D. A. Allison, and K. Siegbahn, Phys. Scr. **3**, 237 (1971).
[19] D. T. Clark and D. M. J. Lilley, Chem. Phys. Lett. **9**, 234 (1971).
[20] M. B. Robin, *Higher Excited States of Polyatomic Molecules* (Academic, New York, 1974), Vol. 1.
[21] W. M. Flicker, O. A. Mosher, and A. Kuppermann, J. Chem. Phys. **64**, 1315 (1976).
[22] W. L. Jorgensen and L. Salem, *The Organic Chemists Book of Orbitals* (Academic, New York, 1973).
[23] *Landolt–Bornstein Structure Data of Free Polyatomic Molecules*, (Springer, Berlin, 1976), New Series II, Vol. 7.
[24] G. Maccagnani, A. Mangini, and S. Pignataro, Tetrahedron Lett. **36**, 3853 (1972).

[25]S. Pignataro, R. D. Marino, G. Distefano, and A. Mangini, Chem. Phys. Lett. **22**, 352 (1973).
[26]A. P. Hitchcock and I. Ishii, J. Electron Spectrosc. Relat. Phenom. (in press).
[27]R. N. S. Sodhi, S. Daviel, C. E. Brion, and G. G. B. de Souza, J. Electron Spectrosc. Relat. Phenom. **35**, 45 (1985).
[28]R. N. S. Sodhi, M.Sc. thesis, University of Alberta, Canada (1981).
[29]R. N. S. Sodhi and C. E. Brion, J. Electron Spectrosc. Relat. Phenom. **34**, 363 (1984).
[30]B. A. Sexton, Surf. Sci. **163**, 99 (1985).